Eur. Phys. J. C 2, 351–358 (1998)

THE EUROPEAN PHYSICAL JOURNAL C
© Springer-Verlag 1998

Hadron production in relativistic nuclear collisions: thermal hadron source or hadronizing quark-gluon plasma?*

C. Spieles[1], H. Stöcker[1], C. Greiner[2]

[1] Institut für Theoretische Physik, J. W. Goethe-Universität, D-60054 Frankfurt am Main, Germany
[2] Institut für Theoretische Physik, J. Liebig-Universität, D-35392 Gießen, Germany

Received: 15 April 1997 / Revised version: 5 June 1997

Abstract. Measured hadron yields from relativistic nuclear collisions can be equally well understood in two physically distinct models, namely a static thermal hadronic source vs. a time-dependent, nonequilibrium hadronization off a quark-gluon plasma droplet. Due to the time-dependent particle evaporation off the hadronic surface in the latter approach the hadron ratios change (by factors of $\lessapprox 5$) in time. Final particle yields reflect time averages over the actual thermodynamic properties of the system at a certain stage of the evolution. Calculated hadron, strangelet and (anti-)cluster yields as well as freeze-out times are presented for different systems. Due to strangeness distillation the system moves rapidly out of the T, μ_q plane into the μ_s-sector. Strangeness to baryon ratios $f_s = 1 - 2$ prevail during a considerable fraction (50%) of the time evolution (i.e. Λ-droplets or even Ξ^--droplets form the system at the late stage: The possibility of observing this time evolution via two-particle correlations is discussed). The observed hadron ratios require $T_c \approx 160$ MeV and $B^{1/4} \gtrapprox 200$ MeV. If the present model is fit to the extrapolated hadron yields, metastable hypermatter can only be produced with a probability $p < 10^{-8}$ for $A \geq 4$.

1 Hadron ratios from an equilibrated source

Measurements of strange and anti-strange particles in relativistic nuclear collisions have received much attention recently [1,2]: (Anti-)strangeness enhancement relative to pp-data has been predicted as quark gluon plasma signal, because equilibrium yields of strange hadrons cannot be achieved during the short collision time due to small $s\bar{s}$ cross sections [3]. However, several thermal models have been applied [4–6] to (strange) particle yields and used to extract the characteristic thermodynamic properties of the system (a few macroscopic parameters) from chemical equilibrium.

Figure 1 shows such a calculation: different measured and calculated hadron ratios are shown as resulting from an equilibrium hadron gas at fixed temperature T, quark chemical potential μ_q and strange quark chemical potential μ_s. The constituents of the hadron gas are all well-established hadrons up to masses of 2 GeV (coinciding with the list given in [7]) taken from [8]. Note that an isospin symmetric system is assumed (as in the hadronization model): #(protons)=#(nucleons)/2, $\#(\pi^+)$=#(all pions)/3 etc. The system is treated as a mixture of relativistic, non-interacting Bose–Einstein and Fermi–Dirac gases with Hagedorn's eigenvolume correction.

The parameters T and μ_q of Fig. 1 are chosen in line with the values given by P. Braun-Munzinger and J. Stachel in [6]. Agreement with many observed ratios from different experiments at the SPS is achieved (as in [6]). The value of μ_s has been determined by the requirement that the total net-strangeness vanishes: $f_s^{init} = 0$. The quantity f_s is the fraction of net-strangeness over net-baryon number ($f_s = (N_s - N_{\bar{s}})/A$). Note that the

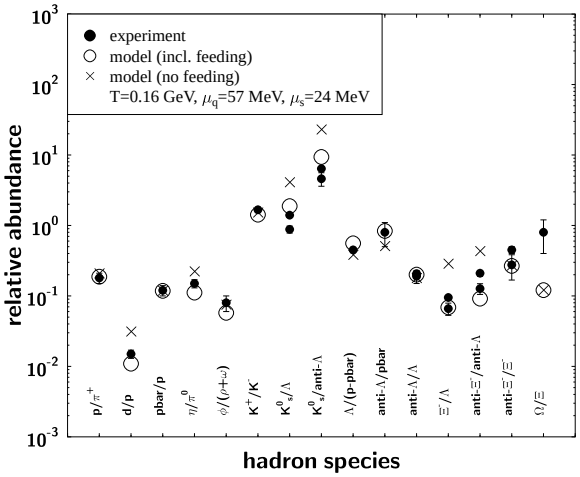

Fig. 1. Particle ratios in the static equilibrium scenario with the parameters (temperature, chemical potentials) as indicated. The *crosses* denote the resulting values if contributions due to the decay of higher lying resonances are ignored. The *circles* include these effects. Data from various experiments as compiled in [6] are also shown

* Supported by GSI, BMBF, DFG

presently calculated strange quark chemical potential $\mu_s = 24$ MeV is different from the value $\mu_s = 18.6$ MeV given in [6]. For the ratios we gain roughly the same results, however, there is a discrepancy of about a factor of 2 in the $\Lambda/(p-\bar{p})$ and $\bar{\Lambda}/\bar{p}$ values.

It should be mentioned that some of the measured ratios may deviate from the true, yet to be observed 4π-ratios: the p/π^+ ratio, which is a rather direct measure of the specific entropy S/A in the fireball, has a value of 0.18(3). However, it is calculated from proton yields in the rapidity range 2.6 to 2.8 and pion yields in the range 3.2 to 4.8 [9]. The $(\Omega^- + \overline{\Omega}^-)/(\Xi^- + \overline{\Xi}^-)$ ratio is measured for $p_t > 1.6$ GeV which excludes a major part of the momentum distributions. If one takes the value for a common m_t-cut (1.7 ± 0.9 for $m_t > 2.3$ GeV [10]) the ratio is compatible with the extracted temperatures and chemical potentials, since within the restricted phase space it is just the ratio of the fugacities times the degeneracies [5], which deviates considerably from the value for the full phase space. However, to allow for a consistent comparison to other models all experimental data are taken from the compilation in [6] and we also give 4π ratios for both presented models.

Figure 1 shows the massive effect (factors of $\gtrapprox 3$!) of feeding on the predicted ratios (cf. the discussion in [11]): the crosses denote the ratios as predicted, if the contributions due to the decay of higher lying resonances (e.g. $\Delta \to \pi + p$, $\rho \to \pi^+ + \pi^-$ etc.) are ignored. The circles show the ratios as obtained after one includes these feeding effects. In some cases both hadron species change considerably due to feeding, but sometimes such that the ratio does not change much, e.g. $(\bar{p}/p)^{eq} \approx \frac{\bar{p}^{eq} + \bar{p}^*}{p^{eq} + p^*}$, where $\bar{p}^*$, p^* denote the yields [11] due to the decay of resonances (e.g. $\bar{\Delta}$, Δ).

Collective motion and fits to particle spectra, respectively, are not considered here. Longitudinal and transverse flow velocities have already been extracted from particle spectra in combination with a static thermal model [12]. However, it is questionable, whether thermal and chemical freeze-out happen simultaneously. Here, we focus on a collective, *chemical* freeze-out.

2 The hadronization model

We now investigate, whether the reasonable agreement of data and model, as reached with the static equilibrium-plus-feeding model, can also be achieved with a dynamic model, which includes the formation and expansion of quark-gluon matter, a first order phase transition into coexistence of quark and hadron matter, and time-dependent evaporation of hadrons from the system, as it evolves with time through the phase transition. This means adopting a model for the hadronization and space-time evolution of quark matter droplets given in [13]. A similar approach was given in [14], however, in terms of rate equations for the flavor kinetics. They allow the abundances of the different constituents of the system to be out of equilibrium, which is in contrast to our model. The calculated hadron yields in both models are similar, if the same initial input is used.

The model [13] assumes a first order phase transition of the QGP to hadron gas with Gibbs conditions ($P^{QGP} = P^{HG}$, $T^{QGP} = T^{HG}$, $\mu_q^{QGP} = \mu_q^{HG}$, $\mu_s^{QGP} = \mu_s^{HG}$) for coexistence. The expansion and evaporation of the system takes into account equilibrium, as well as nonequilibrium features of the process:

1. The plasma sphere is permanently surrounded by a layer of hadron gas, with which it stays in thermal and chemical equilibrium during the phase transition (Gibbs conditions). The strangeness degree of freedom stays in chemical equilibrium between the two phases (however, $< s - \bar{s} > \neq 0$ for the individual phases). Thus, the hadronic particle production is driven by the chemical potentials.
2. The particle evaporation is incorporated by a time-dependent freeze-out of hadrons from the hadron phase surrounding the QGP droplet. During the expansion, the volume increase of the system thus competes with the decrease due to the evaporative, time-dependent freeze–out.

The global properties, like (decreasing or increasing) S/A and f_s of the remaining two-phase system, then change in time according to the following differential equations for the baryon number, the entropy, and the net strangeness number of the total system [13]:

$$\begin{aligned} \frac{d}{dt} A^{tot} &= -\Gamma_1 \, A^{HG} \\ \frac{d}{dt} S^{tot} &= -\Gamma_2 \, S^{HG} \\ \frac{d}{dt} (N_s - N_{\bar{s}})^{tot} &= -\Gamma_3 \, (N_s - N_{\bar{s}})^{HG} \ , \end{aligned} \tag{1}$$

For simplicity, we set $\Gamma_1 = \Gamma_2 = \Gamma_3$, thus, $\Gamma = \frac{1}{A^{HG}} \left(\frac{\Delta A^{HG}}{\Delta t} \right)_{ev}$ is the effective ('universal') rate of particles (of converted hadron gas volume) evaporated from the hadron phase. A more general treatment with differing rates for the three quantities is presently being studied [15].

The equation of state consists of the bag model for the quark gluon plasma and the hadron gas of the previous section. Thus, one solves simultaneously the 'non-equilibrium' dynamics (1) and the Gibbs phase equilibrium conditions for the intrinsic variables, i.e. the chemical potentials and the temperature, as functions of time. Analogously to the static model, there are two free parameters (assuming $f_s = 0$), namely the bag constant $B^{1/4}$ and the initial specific entropy per baryon S/A. These parameters control the initial chemical potentials and the temperature.

3 Particle rates from the hadronizing plasma

The particle yields as functions of time have been calculated for different parameter sets: In Fig. 2 the final (time integrated) ratios are plotted for a bag constant of

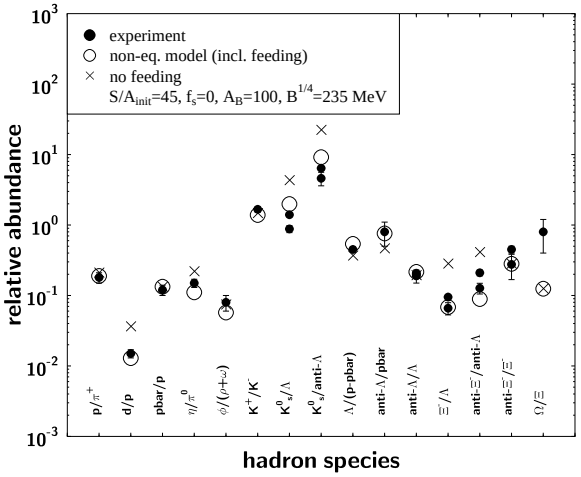

Fig. 2. Final particle ratios in the non-equilibrium scenario with initial conditions $A_{\rm B}^{\rm init} = 100$, $S/A^{\rm init} = 45$, $f_s^{\rm init} = 0$ and bag constant $B^{1/4} = 235$ MeV. The *crosses* denote the resulting values if contributions due to the decay of higher lying resonances are ignored. The *circles* include these effects. Data from various experiments as compiled in [6] are also shown

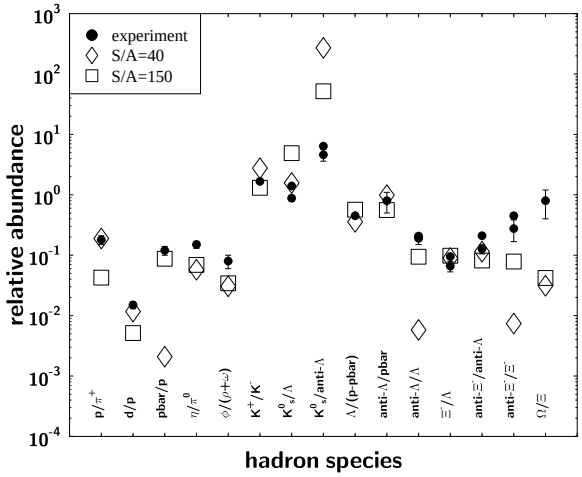

Fig. 3. Final particle ratios (including feeding) in the non-equilibrium scenario with initial conditions $A_{\rm B}^{\rm init} = 100$, $f_s^{\rm init} = 0$ and bag constant $B^{1/4} = 160$ MeV. The initial specific entropy is $S/A^{\rm init} = 40$ (*diamonds*) and $S/A^{\rm init} = 150$ (*squares*), respectively. Data from various experiments as compiled in [6] are also shown

$B^{1/4} = 235$ MeV, initial strangeness fraction $f_s = 0$ and an initial specific entropy per baryon of $S/A = 45$. We choose an initial net-baryon number $A_B^{init} = 100$. The particle ratios do not depend on this choice. (This follows rigorously from the differential equations (1) in the limit that the surface layer is infinitely thin. Numerically on finds that this holds also for finite, but reasonably small thickness of the outer hadron layer [13].) Only the overall time scale changes as $(A_B^{init})^{1/3}$. The theoretical ratios show an equally good overall agreement with the data points as the static fit. This scenario results in a rather rapid hadronization. The quasi-isentropic expansion of the system is due to those hadrons which are subsequently evaporated. Decays and feeding occur after the hadrons leave the system. The specific entropy extracted with this fit is higher than the values given in [16] for this beam energy ($S/A \approx 20 - 25$), where entropy production was calculated in a one-dimensional hydrodynamic model of a heavy ion collision. The calculation of particle rates from a hadronizing QGP with $B^{1/4} = 235$ MeV has already been presented in [13], however, with $S/A^{init} = 25$. Predictions have been also made for different conditions within the rate-equation approach of [14] which yields much higher K/π ratios.

The system can cool within this model (meaning the employed equations of state for both phases) if $(S/A)^{QGP}/(S/A)^{had} < 1$ [13,17], which can only be achieved for a low bag constant. Low bag constants allow for the formation of metastable strange remnants of the plasma, the strangelets. However, the particle yields as resulting from such small B-values in the present model are not in good overall agreement with the observed ratios. This is shown in Fig. 3 where a bag constant of $B^{1/4} = 160$ MeV and an initial specific entropy per baryon of $S/A = 40$ and $S/A = 150$, respectively, is chosen. The results for the lower specific entropy are tolerable except for ratios where antibaryon yields are set in relation to baryon or meson yields. Antibaryon to baryon ratios fail by more than one order of magnitude, which is due to the lower temperatures of the coexistence phase. This is in agreement with the findings of [6] that temperatures much below 160 MeV cannot provide a good description of the data. To counteract this effect, much higher initial specific entropies would be required. However, in particular the ratios p/π^+ and d/p will then move away considerably from the experimentally observed values (see Fig. 3).

Note that within microscopic hadronic model calculations [18] a pronounced dependence of antibaryon (and even more so anti-cluster) yields on the reaction volume has been predicted. This chemical non-equilibrium reflects the strong sensitivity of antibaryon production and absorption on the phase space evolution of the baryons. It is in contradiction to the 'volume freeze-out' of thermal models. On the other hand, even if equilibration of antibaryons is assumed, the abundances are predicted to be strongly enhanced in the case of an *interacting* hadron gas [20].

Figure 4 shows the time evolution of the system (initial conditions as in Fig. 2) in the plane of quark and strange quark chemical potential. The quark chemical potential is at the beginning of the evolution in the order of the temperature of the system. It is $\mu_q \approx 110$ MeV. This is twice the value assumed in the static approach, $\mu_q \approx 60$ MeV. However, in the course of the hadronization, the quark chemical potential drops to $\mu_q \approx 15$ MeV. On the other hand, the strange chemical potential increases from $\mu_s = 0$ to values of $\mu_s \approx 50$ MeV at the end of the evolution, as compared to $\mu_s \approx 25$ MeV in the static fit. This is due to the strangeness distillation effect (see below).

Figure 5 shows the time evolution of the system in the μ_q-T plane in conjunction with the phase diagram of the

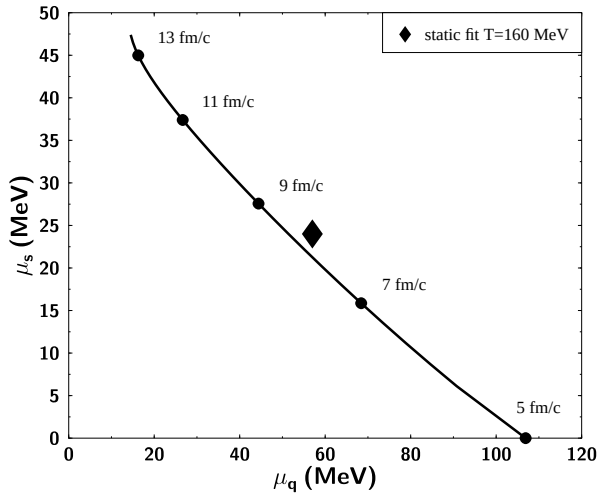

Fig. 4. Time evolution of the quark chemical potential and the strange quark chemical potential for the parameter set of Fig. 2 (here and in the following pictures we start the hadronization at an initial time of $t_0 = 5$ fm/c). The *diamond* denotes the chemical potentials extracted with the static fit (Fig. 1)

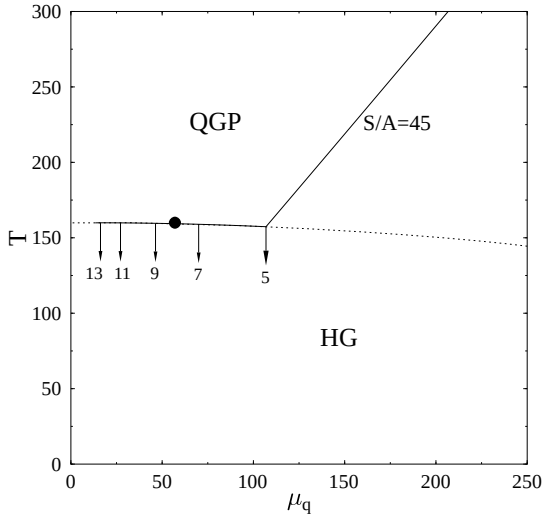

Fig. 5. Hadronization path of the system (initial conditions as in Fig. 2) in the projected $T - \mu_q$ plane. The *numbers* denote the time in fm/c. Shown is also the phase boundary of a QGP and the hadron gas for $B^{1/4} = 235$ MeV and the path of constant specific entropy in a pure quark phase with $S/A = 45$. The *full circle* indicates the μ_q and T values of the static fit

quark gluon plasma phase and the hadron gas. The initial specific entropy of $S/A = 45$ in combination with the bag constant $B^{1/4} = 235$ MeV leads to a fast decomposition of the quark phase within ≈ 13 fm/c. The system moves on a path along the phase boundary. In our case we met the situation $(S/A)^{QGP}/(S/A)^{HG} > 1$ which leads to a reheating, i.e. $(S/A)^{QGP}$ increases with time [13,21,17], to a final value of $S/A \approx 140$. As a consequence the temperature also increases, but only slightly (as can be seen in Fig. 5). For $B^{1/4} = 160$ MeV the system cools, while the specific entropy of the quark drop decreases. In this

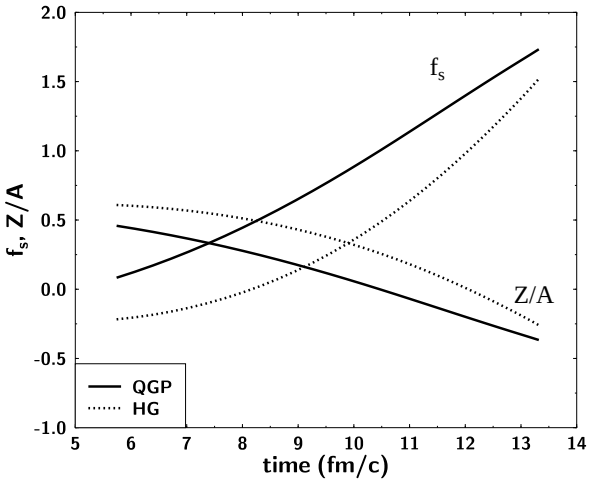

Fig. 6. Time evolution of the QGP and the hadron phase (initial conditions as in Fig. 2). Shown are the strangeness fraction f_s^{QGP}, f_s^{HG} as well as the fraction of charge over baryon number Z/A^{QGP}, Z/A^{HG}

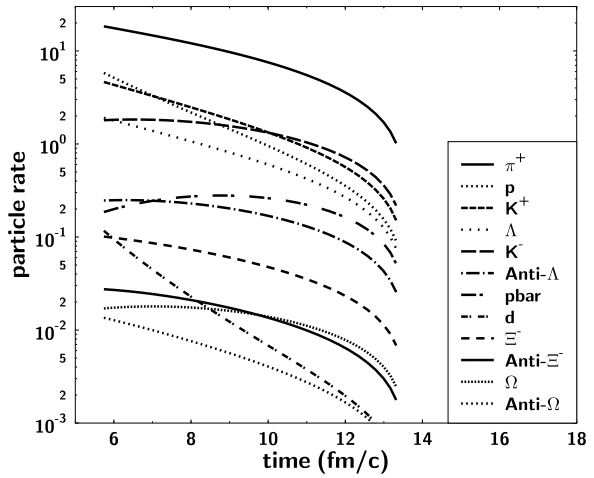

Fig. 7. Particle rates as functions of time (initial conditions as in Fig. 2)

case, the hadronization is incomplete and a strangelet of baryon number $A \approx 8 - 9$ is formed.

Due to the 'strangeness distillery' effect [22] strange and antistrange quarks do not hadronize at the same time for a baryon-rich system: Both the hadronic and the quark matter phases enter the strange sector, $f_s \neq 0$, of the phase diagram immediately. This is valid for both scenarios, the higher bag constant (reheating) as well as the lower bag constant (cooling). The effect can be seen from the high values of the strangeness fraction in the quark phase, shown in Fig. 6 for the higher bag constant $B^{1/4} = 235$ MeV. At the late stage of the evolution, as the strange chemical potential increases, the hadron phase reaches positive f_s values as well. Figure 6 shows also the charge to mass ratio of the two phases.

The rapid expansion of the system leads to changes of the chemical potentials which reflect on the differential hadron production rates. Figure 7 shows the particle rates

dN_i/dt for different hadrons as functions of time for the initial condition $A_B^{init} = 100$, $S/A = 45$, $f_s = 0$ and a bag constant of $B^{1/4} = 235$ MeV (as in Fig. 2). The particle rates decrease in general due to the shrinking of the system, since evaporation is proportional to the surface. However, the differences in the time dependences of different hadron rates are considerable: proton and deuteron rates drop very fast due to the decreasing quark chemical potential, while the antiproton rate even increases (for the same reason). K^- and Ω production profits from the high strange quark chemical potential at the late stage of the evolution.

Figure 8 shows the time evolution of various particle ratios for the same calculation. Most of the ratios – the final values of which are given in Figs. 2 – change by factors $\approx 2-5$ in the course of the hadronization and evaporation. Therefore, the thermodynamic parameters of a certain stage of the evolution, e.g. of the initial stage, cannot be deduced from the final integrated particle ratios in the present model. For the bag constant of $B^{1/4} = 235$ MeV the temperature stays rather constant (which is not required by the model). Therefore, ratios which do not depend directly on the chemical potentials, like η/π^0 and $\phi/(\rho+\omega)$, do not change significantly.

Table 1 shows the absolute abundances of different hadron species for different initial conditions of the hadronizing quark-hadron system. We assume an initial baryon number of $A_B = 208 + 208$ (Pb+Pb). However, the final particle ratios do not depend on this, because the hadrons yields in this model scale with A_B. Thus one can easily renormalize the model prediction for any system size, i.e. the number of participant nucleons. Keep in mind that isospin symmetric systems are assumed. For $B^{1/4} = 235$ MeV the system hadronizes completely, while the specific entropy of the quark phase rises from $S/A^{init} = 30$ (40, 50) to $S/A^{final} = 109$, (130, 153). For $B^{1/4} = 160$ MeV a cold strangelet of mass $A \approx 35$ ($S/A^{init} = 40$) or $A \approx 42$ ($S/A^{init} = 150$) emerges. The table shows that antibaryon yields are very sensitive to the bag constant, whereas the pions depend strongly on the initial specific entropy.

The K/π ratio from the dynamic hadronization and the 'favorable' bag constant of $B^{1/4} = 235$ MeV turns out to be too high (this is also a problem of the static fit). From the preliminary plots in [23] one can read off a K_s^0/h^- ratio of 0.11–0.12 for central Pb+Pb collisions (4π yields), whereas the model yields a value of $K_s^0/h^- \approx 0.15$ for the three choices of initial specific entropy. It is possible to improve this ratio by assuming a lower bag constant. For $B^{1/4} = 160$ MeV the model renders K_s^0/h^- ratio of ≈ 0.1, as can be seen in Table 1. It can be argued that the numbers of kaons and pions as the most abundant particles reflect the actual thermodynamic conditions much more accurately than other hadron species.

Figure 9 shows calculated multiplicities of various hypermatter clusters for $B^{1/4} = 235$ MeV, $A_B = 416$ and $S/A = 40$. The penalty factor $\sim e^{(\mu-m)/T}$ suppresses the abundances of heavy clusters during the hadronization process, which is reflected by the final yields: metastable hypermatter can only be produced with a probability $p < 10^{-8}$ for $A \geq 4$ (e.g. a $\{2\Xi^-, 2\Xi^0\}$ object).

Can one discriminate the static thermal and the hadronizing source from observations of hadron abundances? Obviously, the final particle ratios are nearly identical and therefore not suitable for discriminating the two scenarios. The strong change in the time dependent particle rates (Fig. 8) reflects different average freeze-out times of the particle species. These, in turn, correspond to different average freeze-out radii, since the quark drop shrinks — in this scenario — during the hadronization process. Both quantities, which characterize the size and the lifetime of the particle emitting source, are in principle accessible by means of Hanbury-Brown-Twiss-analyses [24]. This concept is used extensively for high energy heavy ion collisions (for a review see [25]). However, it is difficult to separate the spatial and temporal structure of the emitting source by this method, since emission with a larger radius, but over a shorter time span can give the same signal as emission over a longer time with smaller radii. Furthermore, HBT cannot measure the absolute time of the emission but only the temporal spread. As an alternative approach, correlations of non-identical particles have been already studied in [19] in order to determine directly the delays in the emission of K^+ and K^-. However, it cannot be concluded yet if the effect is strong enough to be measurable experimentally.

In Table 2 the average freeze-out times of different hadron species resulting from a hadronizing QGP drop (for different initial conditions) are listed. Only the directly produced hadrons are taken into account. The true freeze-out times are generally larger due to the finite lifetime of the resonances, which contribute to specific hadron yields. However, the two-particle correlations within the source — imposed by the quantum statistical momentum distributions — are lost through these decays. Thus, the measured correlation function does not represent a simple Fourier-like transform of the particle distribution inside the emitting source, if the contributions from resonance decays are dominant. As can be seen from Table 2 only a fraction of the integrated, final yield of protons, kaons and pions are directly emitted from the hadronizing system. A major part stems from the decay of higher resonances. This makes the accessibility of the freeze-out radii or times by means of HBT analysis questionable. However, the presented results suggest that the observed freeze-out time will be smaller for K^+ than for K^-, and it will also be smaller for p and Λ than for $\bar{p}$ and $\bar{\Lambda}$, respectively. The corresponding radii behave the opposite in this model, because the system shrinks.

4 Conclusion

Experimental particle ratios at SPS energies are compatible with the scenario of a static thermal source in chemical equilibrium [6]. A simple dynamic hadronization model, however, reproduces the numbers equally well. It yields the following conclusions: a high bag constant of $B^{1/4} \geq 200$ is mandatory. These values of B would exclude the

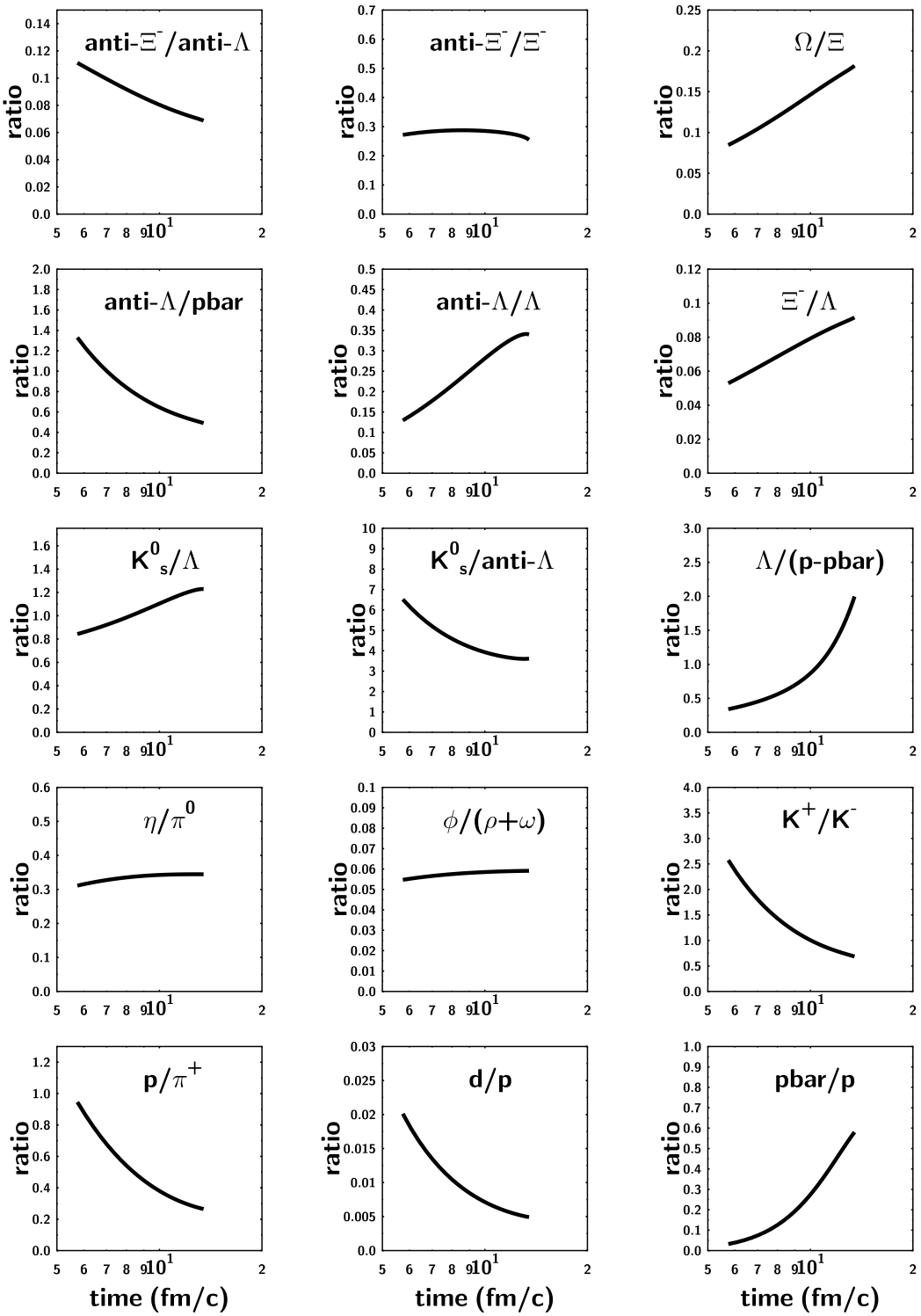

Fig. 8. Time evolution of various particle ratios (including feeding) for the parameter set of Fig. 2. Here the ratios of the *particle rates* at a certain time t are depicted

existence of stable, cold strangelets, as hadronization proceeds without any cooling but with reheating. In central collisions of S+Au(W,Pb) a specific entropy per baryon of $S/A = 35 - 45$ is created. Due to strangeness distillation the system moves rapidly out of the T, μ_B plane, into the μ_s-sector. The quark chemical potential drops during the evolution, the strange quark chemical potential rises. Final μ_q, μ_s values of 1/3 resp. 3 of the values of the static fits are reached for $t \to t_{freeze-out}$. We have presented the model calculations of absolute yields of different hadron species for Pb+Pb collisions at SPS energies. The average freeze-out times of different hadron species

Table 1. Hadron abundances for Pb(160GeV/u)Pb ($A_B^{init} = 416$, $f_s = 0$) and different initial conditions of the hadronizing quark drop. The numbers for the total yields (including feeding from higher resonances) are given

S/A^{init}	$B^{1/4}$ (MeV)	p	π^+	d	$\bar{p}$	ϕ	ρ	ω	K^+
30	235	173.7	619.3	4.3	11.3	12.9	176.6	56.0	130.0
40	235	180.0	852.2	2.8	20.0	18.8	248.9	81.2	175.4
50	235	188.7	1084.5	2.2	30.2	24.6	320.7	106.2	219.2
40	160	150.7	798.9	1.8	0.3	2.7	68.9	20.8	124.6
150	160	149.7	3522.0	0.8	13.1	17.6	390.5	122.2	430.3
		K^-	K_s^0	Λ	$\bar{\Lambda}$	Ξ^-	$\bar{\Xi}^-$	Ω	$\bar{\Omega}$
30	235	81.8	105.9	67.6	8.6	4.4	0.81	1.00	0.30
40	235	122.3	148.8	79.8	15.0	5.4	1.3	1.3	0.49
50	235	163.4	191.3	90.5	22.5	6.4	2.1	1.6	0.70
40	160	44.8	84.7	53.8	0.3	4.9	0.04	0.3	0.01
150	160	328.7	379.5	77.6	7.4	7.7	0.6	0.6	0.01

Table 2. Average freeze-out times (in fm/c) of different hadron species for Pb(160GeV/u)Pb ($A_B^{init} = 416$, $f_s^{init} = 0$). The results for different initial specific entropies of the hadronizing quark drop are shown. The fraction of directly produced hadrons divided by the total yield (including feeding) is given in brackets

S/A^{init}	$B^{1/4}$ MeV	p	π^+	d	$\bar{p}$	K^+	K^-
30	235	3.3 (.36)	4.8 (.30)	2.1 (1.0)	7.1 (.36)	4.2 (.55)	6.0 (.51)
40	235	4.1 (.36)	5.6 (.32)	2.9 (1.0)	7.6 (.36)	5.0 (.54)	6.6 (.51)
50	235	4.8 (.35)	6.2 (.32)	3.5 (1.0)	8.1 (.35)	5.6 (.53)	7.1 (.51)
		Λ	$\bar{\Lambda}$	Ξ^-	$\bar{\Xi}^-$	Ω	$\bar{\Omega}$
30	235	4.3 (.24)	5.8 (.21)	5.1 (.98)	5.2 (.97)	6.1 (1.0)	4.3 (1.0)
40	235	5.1 (.24)	6.4 (.21)	5.8 (.98)	5.8 (.97)	6.8 (1.0)	5.0 (1.0)
50	235	5.8 (.24)	6.9 (.22)	6.4 (.98)	6.4 (.97)	7.3 (1.0)	5.6 (1.0)

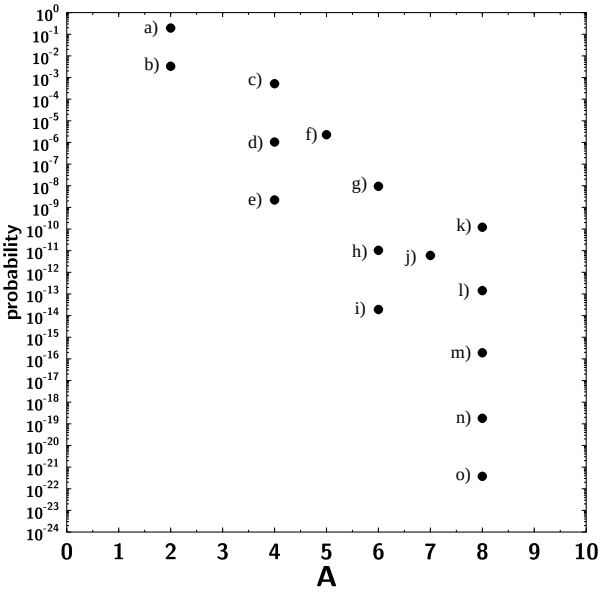

Fig. 9. Calculated multiplicities of hypermatter clusters from a hadronizing QGP with $A_B^{init} = 416$, $S/A^{init} = 40$, $f_s^{init} = 0$ and a bag constant of $B^{1/4} = 235$ MeV:
a) H^0 (m = 2020 MeV), b) $\{\Xi^-, \Xi^0\}$, c) ${}^4He$, d) $\{4\Lambda\}$, e) $\{2\Xi^-, 2\Xi^0\}$, f) ${}^5_{\Lambda}He$, g) ${}^6_{\Lambda\Lambda}He$, h) $\{2n, 2\Lambda, 2\Xi^-\}$, i) $\{2\Lambda, 2\Xi^0, 2\Xi^-\}$, j) ${}^7_{\Xi^0\Lambda\Lambda}He$, k) $A = 8$, $S = 0$, l) $A = 8$, $S = -4$, m) $A = 8$, $S = -8$, n) $A = 8$, $S = -12$, o) $A = 8$, $S = -16$
($-S$ gives the number of strange quarks)

differ strongly, which might be observable via two-particle correlation analyses. Strangeness to baryon fractions of $f_s \approx 1 - 2$ suggest that 'Λ-droplets' or even 'Ξ^--droplets' form the system at the late stage.

Acknowledgements. We thank Dieter Röhrich, Reinhard Stock, Johanna Stachel, Peter Braun-Munzinger, Johannes Wessels and Helmut Satz for fruitful discussions.

References

1. Proc. of the XI. Int. Conf. on Ultrarelativistic Nucleus-Nucleus Collisions, Quark Matter '95, Monterey, CA, USA, Nucl. Phys. A **590**, (1995); Proc. Int. Conf. on Nuclear Physics at the Turn of the Millenium: Structure of Vacuum and Elementary Matter, 10-16 March 1996, Wilderness/George, South Africa, World Scientific Publ. Co., Singapore (1997); Proc. of the XII. Int. Conf. on Ultrarelativistic Nucleus-Nucleus Collisions, Quark Matter '96, Heidelberg, Germany,Nucl. Phys. A **610**, (1996)
2. International Symposium on Strangeness and Quark Matter (Sept. 1-5, 1994) Crete (Greece) World Scientific, 1995; Proc. of the Int. Conf. on Strangeness in Hadronic Matter, Tucson, AZ, USA, AIP Press, Woodbury, NY (1995)
3. P. Koch, B. Müller, J. Rafelski, Phys. Rep. **142**, 167 (1986)
4. J. Cleymans and H. Satz, Z. Phys. C **57**, 135 (1993)
5. J. Letessier, A. Tounsi, U. Heinz, J. Sollfrank, J. Rafelski, Phys. Rev. D **51**, 3408 (1995)

6. P. Braun-Munzinger, J. Stachel, J.P. Wessels, N. Xu, Phys. Lett. B **344**, 43 (1995); P. Braun-Munzinger, J. Stachel, J.P. Wessels, N. Xu, Phys. Lett. B **365**, 1 (1996); P. Braun-Munzinger and J. Stachel, Nucl. Phys. A **606**, 320 (1996)
7. L.A.Winckelmann et al., Nucl. Phys. A **610**, 116 (1996)
8. Particle Data Group, Phys. Rev. D **54**, 1 (1996)
9. M. Murray for the NA44 Collab., Nucl. Phys. A **566**, 515 (1994)
10. D. Di Bari and the WA85 Collab., Nucl. Phys. A **590**, 307 (1995)
11. H. Stöcker, J. Phys. G **10**, L111 (1984); D. Hahn and H. Stöcker, Nucl. Phys. A **452**, 723 (1986) Nucl. Phys. A **476**, 718 (1988)
12. J. Stachel, Nucl. Phys. A **610**, 509 (1996)
13. C. Greiner and H. Stöcker, Phys. Rev. D **44**, 3517 (1991)
14. H.W. Barz, B.L. Friman, J. Knoll and H. Schulz, Nucl. Phys. A **484**, 661 (1988); Phys. Rev. D **40**, 157 (1989)
15. A. Dumitru, C. Spieles, H. Stöcker, C. Greiner, manuscript in preparation
16. D.H. Rischke, B.L. Friman, H. Stöcker, W. Greiner, J. Phys. G **14**, 191 (1988); D.H. Rischke, B.L. Friman, B.M. Waldhauser, H. Stöcker, W. Greiner, Phys. Rev. D **41**, 111 (1990)
17. C. Greiner, J. Schaffner, *Quark Gluon Plasma 2*, ed. R.C. Hwa, World Scientific (1995), p. 635
18. A. Jahns, C. Spieles, R. Mattiello, H. Stöcker, W. Greiner , H. Sorge, Phys. Lett. B **308**, 11 (1993); M. Bleicher, C. Spieles, A. Jahns, R. Mattiello, H. Sorge, H. Stöcker, W. Greiner, Phys. Lett. B **361**, 10 (1995)
19. S. Soff et al., in Proc. of the Int. Symposium on "Strangeness in Quark Matter 1997", Thera (Santorini), Greece, April 14-18 (1997), to be published in J. Phys. G
20. J. Schaffner, I.N. Mishustin, L.M. Satarov, H. Stöcker, W. Greiner, Z. Phys. A **341**, 47 (1991)
21. P. R. Subramanian, H. Stöcker, W. Greiner; Phys. Lett. B **173**, 468 (1986)
22. C. Greiner, P. Koch and H. Stöcker, Phys. Rev. Lett. **58**, 1825 (1987); C. Greiner, D. H. Rischke, H. Stöcker and P. Koch, Phys. Rev. D **38**, 2797 (1988)
23. P.G. Jones and the NA49 Coll. Nucl. Phys. A **610**, 188 (1996)
24. R. Hanbury-Brown and R.Q. Twiss, Nature **178**, 1046 (1956)
25. B.V. Jacak, for the NA44 Coll., Nucl. Phys. A **590**, 215 (1995)